Proceedings 10th NUMGE 2023
10th European Conference on Numerical Methods in Geotechnical Engineering
Zdravkovic L, Kontoe S, Taborda DMG, Tsiampousi A (eds)

https://doi.org/10.53243/NUMGE2023-257

Numerical study on the behaviour of earthen embankment built on liquefiable soil

Abhijit Chakraborty[1], V. A. Sawant[1]

[1]*Department of Civil Engineering, IIT Roorkee, Uttarakhand, India, 247667*

ABSTRACT: The present study is concerned with the liquefaction behaviour of foundation soil resting beneath the embankment and the effects of liquefaction on the behaviour of the embankment. The FEM-based PLAXIS 2D application is used for simulation while assuming plane strain conditions. Using the UBC3D-PLM constitutive model, loose, cohesionless foundation soil has been modelled. The variation of embankment response has been explored with the variation of the relative density of foundation soil. It has also been investigated that with increasing cyclic loading amplitude embankment crest settlement increases. With the increase in the relative density of foundation soil, embankment crest settlement reduces by 48.48%, 30.65%, and 24.76% in the case of 0.1g, 0.2g, and 0.3g cyclic loading amplitudes, respectively. The toe region exhibits complete liquefaction within a few cycles of loading which mostly contributes to the settlement of the embankment. Later, a seismic analysis for various ground motions was carried out. A linear relationship between embankment settlement and arias intensity of ground motions has been observed. It may be inferred from the untreated embankment model that mitigation of the foundation soil beneath the toe can be a successful strategy in preventing liquefaction-induced settlement.

Keywords: Liquefaction; Relative Density; Embankment Settlement; Lateral Outflow; UBC3D-PLM Model

1 INTRODUCTION

During previous major earthquakes, damage to earthen dams, dikes, and road embankments was reported. Yamada (1966), McCulloch and Bonilla (1967), Matsuo (1996), Adalier et al. (1998), and other earlier investigations have provided deeper insights into the catastrophic damage to earthen embankments due to liquefaction of foundation soil. A neighbouring densely inhabited area was flooded as a result of the Lower Van Norman Dam's massive fall caused by liquefaction (NRC 1985), which happened during the 1971 San Fernando earthquake. Due to the development of excess pore pressure in the foundation soil, a 140 feet high dam lost its shear strength and began to sink. Following the 1995 Osaka-Kobe earthquake, similar destruction of embankment constructions was also recorded. Adalier (1996) concluded from the extensive dynamic centrifuge investigation that the soil beneath the embankment's toe and in front of it develops substantial excess pore pressure (EPP). The foundation soil tries to shift sideways away from the center line of the embankment as a result of increasing sideways shear stresses due to relative lateral movement between the embankment and foundation soil at the interface. Consequently, there is significant deformation, and the soil nearby begins to lose its shear strength. However, due to the difficulty and expense of such a study, numerical modeling emerges as a viable substitute. In the recent few decades, there has been significant progress in the field of soil constitutive models for sands (Yang et al. 2003; Taiebat and Dafalias 2008; Andrianopoulos et al. 2010; Boulanger and Ziotopoulou 2013). Past studies (Dinesh et al. 2022; Chakraborty and Sawant 2022a) have shown that by using calibrated parameters of an advanced constitutive model, reliable analysis can be carried out. The present study behaviour of embankment built on saturated cohesionless soil under dynamic loading has been investigated. A well-calibrated effective stress-based dynamic constitutive material model UBC3D-PLM has been used for simulating the liquefaction behaviour of sandy foundation soil. The detailed calibration methodology of the UBC3D-PLM material model has been avoided in this study and can be found in past studies (Chakraborty and Sawant 2022a, 2022b).

2 METHODOLOGY

The finite element method-based program PLAXIS 2D has been used in the present study for the analyses. The entire model domain has been discretized by 15-node 2D triangular elements. A similar type of interpolation function is used for finding out both the displacements and pore pressures. PLAXIS 2D uses an implicit Newmark time integration scheme for solving the dynamic equilibrium equation. During dynamic loading conditions, a dynamic viscous boundary has been considered for simulating the far field condition and for avoiding the

spurious reflection of waves inside the soil domain. Viscous boundaries, which also incorporate the Neumann type of boundary condition, update the stresses at the boundary by nullifying the reflected stresses. A similar boundary condition has been adopted in past studies (Bhatnagar et al. 2016; Chakraborty and Sawant 2022a, 2022b).

3 MODEL GEOMETRY AND DETAILS

Figure 1 shows the geometry of the embankment and foundation soil layer configuration details. The embankment is considered to be 4.5 m high with 1:1 side slopes and 5.63 m top width. Whereas the foundation soil has been considered to be of two different layers, where the top layer is prone to liquefaction and the bottom layer is a dense sand layer.

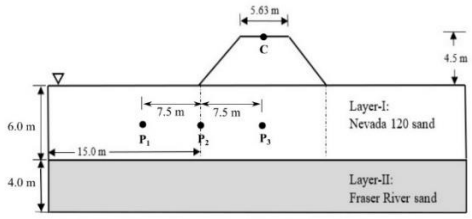

Figure 1. Embankment model geometry

Layer I have been chosen to be Nevada 120 sand (40% and 60%) to investigate the effect of R_D of the foundation sand layer on the embankment response. Layer II is considered as Fraser river sand of R_D = 80%. Layer I and Layer II have a depth of 6.0 m and 4.0 m, respectively. The embankment material has been modeled using the Mohr-Coulomb material model. Plain strain 2D modeling has been done for the geometry mentioned above to study the embankment behaviour. The dynamic loading has been applied horizontally along the base of the model.

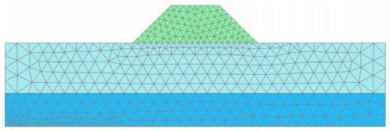

Figure 2. Finite element mesh of embankment model

Figure 2 shows the finite element mesh of the model considered in the present study. Mohr-Coulomb material properties have been considered in the analyses to generate initial stress conditions. A similar strategy has been adopted in the past literature (Dinesh et al. 2022; Chakraborty and Sawant 2022 a).

4 MATERIAL PROPERTIES

The earthen embankment is considered to be made of a mixture of Nevada sand and Kaolin Clay (4:1 by weight ratio). The foundation liquefiable sandy soil properties have been considered based on two different relative densities (R_D = 40% and 60%) of Nevada 120 sand. However, below the liquefiable soil layer, there exists a dense sand layer (R_D = 80%). Liquefiable layer basic properties are taken as Nevada 120 sand properties, from the study of Arulmoli et al. (1992). The dense sand layer's basic properties are taken as Fraser river sand from the study of Sriskandakumar (2004). Properties of embankment material and foundation sandy layers are given in Table 1 and Table 2, respectively.

Table 1. Properties of foundation soil layers

Properties	**Nevada 120 sand**		**Fraser river sand**
R_D	40%	60%	80%
G	2.67	2.67	2.71
γ_{dry} (kN/m^3)	15.08	15.76	16.73
k (m/s)	6.6×10^{-5}	5.6×10^{-5}	5.5×10^{-6}
e_{max}	0.887	-	0.94
e_{min}	0.511	-	0.62

Table 2. Properties of embankment material

Properties	**Embankment clayey sand**
E (MPa)	20
γ_{dry} (kN/m^3)	19
$\gamma_{saturated}$ (kN/m^3)	21
$e_{initial}$	0.50
c (kPa)	22
ϕ (°)	31
k (m/s)	6.94×10^{-6}

5 BEHAVIOUR OF UBC3D-PLM MODEL

UBC3D-PLM is an effective stress-based elastoplastic material model for sand (Pubela et al. 1997, Beaty and Byrne 1998), to simulate liquefaction behaviour under the application of dynamic loading. The model employs the Mohr-Coulomb yield condition in 3-D primary stress space. The hardening rule is governed by the mobilized friction angle (ϕ_{mob}) and plastic shear strain, which is based on the Duncan-Chang method and classical plasticity theory. Non-associative flow rule of this model follows the Drucker-Prager plastic potential function. Petalas and Galavi (2013) provided an empirical correlation between the corrected SPT number [$(N_1)_{60}$] and the UBC3D-PLM model parameters. Parameters K_B^e, K_G^e and K_G^p are the stiffness parameters which mainly control the non-linear stress dependency of stiffness using power coefficients m_e , n_e, and n_p. The failure ratio (R_f) is considered within the range of 0.5 to 1.0. Parameters $f_{ac,hard,}$ and $f_{ac,post}$ govern the densification and post-liquefaction behaviour of saturated sand. In order to maintain the brevity of the paper, only a brief introduction is given, and a detailed description of the model can be

found in the literature (Tsegaye, 2010; Petalas and Galavi, 2013). In a recent study, Chakraborty and Sawant (2022a) showed that the model parameter K_G^p primarily controls liquefaction behaviour. Based on the best-fit liquefaction strength curve against the study of Idriss and Boulanger (2008), this parameter has been fixed for a particular state of sand.

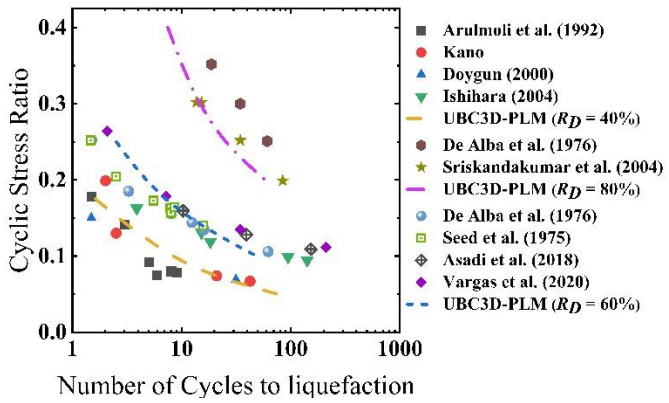

Figure 3. Liquefaction strength curve for different sands

Figure 3 shows the cyclic stress ratio (CSR) vs. the number of cycles of loading required to achieve r_u = 95% or the shear strain of 1.5% for different sands considered in this study. All the sands are K_0 consolidated, which are subjected to zero initial static shear stress ($\alpha = 0$) and 100 kPa initial effective vertical stress (σ'_{v0}). Based on this calibration process, UBC3D-PLM model parameters are given in Table 3.

Table 3. UBC3D-PLM model parameters for different sands

Parameters	R_D (%)		
	40	60	80
ϕ_p (°)	33.65	34.32	38.9
ϕ_{cv} (°)	33	-	-
K_B^e	566.6	717.4	937.6
K_G^e	809.4	1024.8	1339.5
K_G^p	350	635.68	3597.1
m_e	0.5	-	-
n_e	0.5	-	-
n_p	0.4	-	-
R_f	0.83	0.75	0.66
$f_{ac,hard}$	0.45	-	-
$f_{ac,post}$	0.1	-	-
$(N_1)_{60}$	6.5	13.2	29.7

The parameters reported in Table 3 also confirm the stress-controlled cyclic shear tests, which are being avoided to maintain the brevity of the study. However, the detailed calibration process can be found in the study by Chakraborty and Sawant (2022a). These model parameters (Table 3) are used in the present study to simulate the liquefaction behaviour of foundation sandy soil of different R_D and to evaluate the dynamic response of embankment resting on the liquefiable soil deposit.

6 RESULTS AND DISCUSSIONS

Analyses have been carried out initially for cyclic loading conditions and later for earthquake input motion. Accordingly, this section has been divided into two following subsections.

6.1 Response under cyclic loading

To evaluate the response of earth embankment on liquefiable soil deposit under cyclic loading conditions, 10 cycles of harmonic loading of 1.6 Hz frequency have been applied. To evaluate the effect of cyclic loading amplitude (PGA_{cyclic}), three different amplitudes of 0.1g, 0.2g, and 0.3g have been applied at the base of the model.

Figure 4 shows the time-history plots of embankment crest settlement under different levels of PGA_{cyclic} for two different foundation soil conditions (40% and 60% R_D). It is obvious to observe that with the increase in cyclic loading amplitude, the embankment crest settlement also increases. However, higher settlement is observed in the case of foundation soil with 40% R_D in comparison to the soil with 60% R_D.

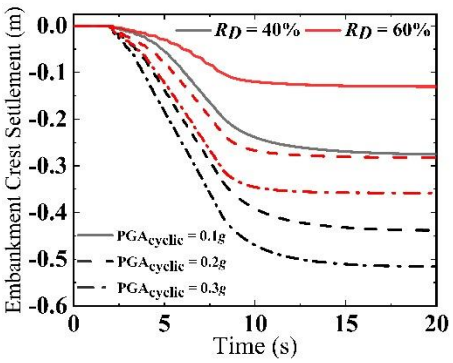

Figure 4. Embankment crest settlement under cyclic loading

For foundation soil of R_D = 40%, 0.198 m embankment crest settlement has been observed at the end of cyclic loading under 0.1g amplitude., The same has been increased to 0.336 m and 0.412 m under 0.2g and 0.3g amplitudes, respectively.

However, with an increase in relative density of foundation soil from loose (R_D = 40%) to medium (R_D = 60%) condition, the embankment crest settlement values for 0.1g, 0.2g, and 0.3g PGA_{cyclic} values are reduced by 48.48%, 30.65%, and 24.76%, respectively. It is observed that with the increase in foundation soil R_D the embankment settlement reduces noticeably. Figure 5 shows the excess pore pressure ratio (r_u) time-history at different locations (P_1, P_2, and P_3) shown in Figure 2 for different R_D values of foundation liquefiable soil for PGA_{cyclic} = 0.1g. These locations are considered based on the past literature (Adalier, 1996). It can be observed that the foundation soil liquefies earlier in the case of R_D = 40%, and the free field of foundation soil (P_1) liquefies after 6.26 cycles of loading.

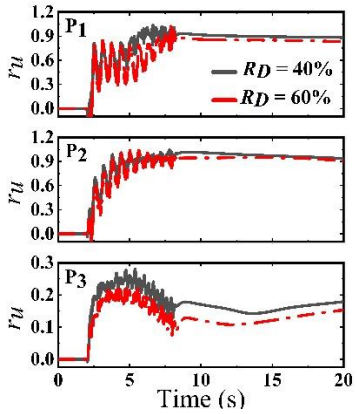

Figure 5. r_u time-history at different locations in the foundation layer PGA_{cyclic} = 0.1g

Whereas, in the case of R_D = 60%, liquefaction at point P_1 occurred after 9.33 cycles of loading. This shows resistance to liquefaction due to the increased relative density (R_D) of sandy foundation soil. Location P_2, below the embankment toe, was found to be more vulnerable to liquefy much earlier than free field condition. In the case of R_D = 40% of the foundation soil, the location P_2 was found to be liquefied within 2.86 cycles of loading, whereas, for R_D = 60%, it took 3.78 cycles to liquefy. This clearly shows that the toe region is much more prone to liquefaction and responsible for the settlement of embankment. This is also reported in a past study by Chakraborty and Sawant (2022a). This indicates mitigation strategy should be considered in the regions below the embankment toes. However, the central foundation soil below the embankment was found to be never reaching the liquefaction condition and provides stability to the embankment. It is observed that in the case of R_D = 40% of the foundation soil, the location below the embankment (P_3) achieves a maximum value of r_u = 0.293. Whereas, in the case of R_D = 60% of the foundation soil, the r_u value is observed to be reduced by 19.11%.

6.2 Response under earthquake loading

To evaluate the response of the embankment-liquefiable foundation soil system under real ground motions. Ten different ground motions have been selected from the PEER ground motion database with a variety of ranges of arias intensity (I_a). The most significant synthetic parameter, Arias Intensity (Ia), of an input ground motion has been chosen to reflect three crucial major ground motion properties, including the motion's amplitude, frequency content, and duration (Kramer 1996). Past studies (Wang, 2012; Huang and Wang, 2017; Cascone et al., 2021, Chakraborty and Sawant, 2022b) have shown that arias intensity (I_a) is an efficient parameter to represent record-to-record variability of response under different ground motions.

Table 4 shows the details of 10 ground motions chosen for the present study containing the station details along with important ground motion parameters (PGA, frequency, and arias intensity).

Table 4. Selected ground motions for the seismic analyses

EQ	Station (Year)	PGA (m/s^2)	f (Hz)	I_a (m/s)
Chi-chi	CHY092 (1999)	1.77	0.70	0.96
Imperial Valley	Aeropuerto, Mexicali (1979)	1.67	2.36	1.22
Kocaeli	Arcelik (1999)	2.16	5.36	0.29
Loma Gilroy	Gilroy Array #2 (1989)	1.67	3.94	0.44
Northridge	Bell Gardens, Jaboneria (1994)	2.16	5.01	0.23
El-Centro	El Centro, Los Angeles (1940)	2.06	2.49	0.84
Coyote	Gilroy Array #1 (1979)	1.22	2.40	0.12
Nahanni	Nahanni Site #3 (1985)	1.47	16.06	0.28
Parkfield	Cholame-Shandon Array#8 (1966)	3.53	2.63	0.45
Whittier Narrow	Beverly Hills-14145 Mulhol (1987)	1.86	6.41	0.26

Figure 6 shows 5% damped response spectra plot of 10 ground motions. Figure 7 shows the variation of dynamic shear stress along the depth of the liquefiable foundation soil layer right under the toe of the embankment. It can be seen that with the increasing depth, the shear stress also increases for 10 selected ground motions. Dynamic shear stress signifies the maximum shear stress during dynamic loading at a particular depth. If it exceeds shear resistance based on prevailing effective stress at that time, soil liquefies. Based on the time-history analyses of 10 different ground motions, it can be observed that there is a linear correlation present between the earthquake-induced embankment crest settlement and arias intensity (I_a) of ground motion.

Final embankment crest settlement in the case of R_D = 40% of foundation liquefiable soil is found to be more than the case of foundation soil with R_D = 60%. Out of 10 different ground motions, maximum embankment crest settlement (with R_D = 40% of foundation soil) can be observed in the case of Imperial Valley ground motion (I_a = 1.22). Figure 8 shows the typical stress-

strain response of P_1, P_2, and P_3 locations of foundation soil (R_D = 40%) under different earthquake loading.

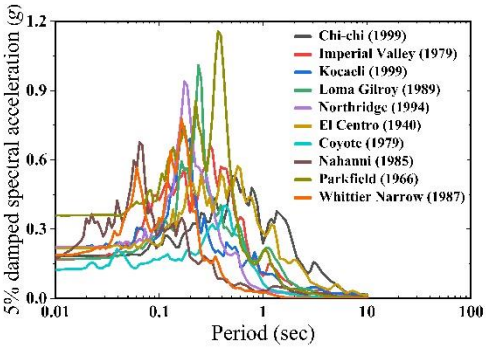

Figure 6. Response spectra of earthquake motions considered in the analyses

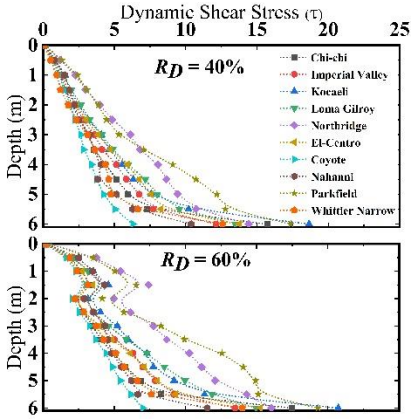

Figure 7. Variation of dynamic shear stress along the depth of liquefiable foundation soil layer

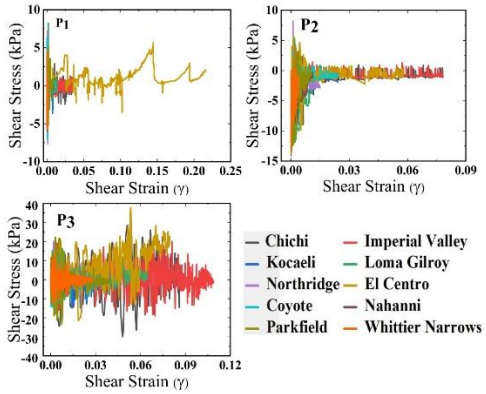

Figure 8. Stress-strain behaviour of P1, P2 and P3 locations during earthquakes (R_D = 40%)

With an increase in foundation soil relative density to 60%, 24.07% reduction in embankment crest settlement can be observed in the case of Imperial Valley ground motion. The minimum settlement has been observed in the case of 1985 Nahanni ground motion (I_a = 0.12), which has the maximum predominant frequency, in which a 39.63% reduction in embankment crest settlement has been observed with an increase in the relative density of sandy foundation soil. However, the maximum reduction (48.60%) of embankment crest settlement by increasing the relative density of foundation soil can be seen in the case of the 1999 Kocaeli ground motion. Table 5 shows the details of the final embankment crest settlement for both the relative density of foundation soil.

Figure 9 shows the plot for the relationship between the embankment crest settlement and the arias intensity (I_a) of ground motion. A linear relationship has been observed with R^2 value of more than 0.97 for both the foundation soil conditions.

$$Settlement = 0.7262 \times Ia \quad (1)$$

$$Settlement = 0.5245 \times Ia \quad (2)$$

Table 5. Details of earthquake-induced final embankment crest settlement

Ground Motion	***RD* (%)**		**% *reduction***
	40	**60**	
Chi-chi	0.662	0.491	25.76
Imperial Valley	0.913	0.693	24.07
Kocaeli	0.286	0.147	48.60
Loma Gilroy	0.401	0.244	39.12
Northridge	0.232	0.131	43.64
El-Centro	0.593	0.458	22.71
Coyote	0.192	0.103	46.25
Nahanni	0.109	0.066	39.63
Parkfield	0.257	0.144	44.13
Whittier Narrow	0.156	0.088	43.55

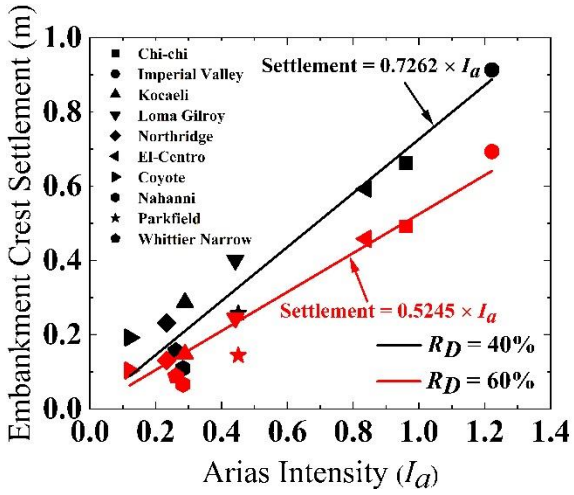

Figure 9. Relationship between arias intensity (I_a) and embankment crest settlement

Equations (1) and (2) represent linear relationships between the embankment settlement and arias intensity

for foundation soil relative density of 40% and 60%, respectively.

These equations can provide valuable input in the case of pseudo-static analysis of embankment or levee structures with similar embankment geometry.

7 ACKNOWLEDGEMENTS

The authors acknowledge the following contributions: Chakraborty, A: Conceptualization, Investigation, Software, Validation, Writing - original draft and Sawant, V.A: Conceptualization, Methodology, Supervision, Writing – review & editing.

8 CONCLUSIONS

The present study highlights key aspects of an embankment built on a liquefiable deposit. Effective stress-based elasto-plastic constitutive model UBC3D-PLM has been adopted to evaluate the dynamic response of an earthen embankment. It has been observed that with increasing foundation soil relative density, the stability of the embankment is increased. Foundation soil below the embankment toe region is more prone to liquefaction and has been found to be liquefying within a few initial cycles of loading. This shows that mitigation strategies for such embankment structures should be focused on the region below the embankment toes. However, it is also observed that the foundation soil beneath the embankment crest never attains the liquefaction condition (r_u = 1.0) and which shows that the UBC3D-PLM model can effectively simulate the beneficial aspect of shear-induced dilation. However, from the seismic study, it can be seen that a linear relation exists between the embankment crest settlement and the arias intensity of ground motions. Moreover, crest settlement for different ground motions is reported, which along with the settlement vs. arias intensity relationships, can be useful for pseudo-static analysis of embankment or levee structures.

9 REFERENCES

Adalier, K. 1996. Mitigation of Earthquake-induced Liquefaction Hazards, *Doctor of Philosophy thesis*, Rensselaer Polytechnic Institute, Troy, New York.

Adalier, K., Elgamal, A.W., and Martin, G.R. 1998. Foundation liquefaction countermeasures for earth embankments, *J. Geotech Geoenviron Eng.* 124(6):500-17.

Andrianopoulos, K.I., Papadimitriou, A.G., Bouckovalas, G.D. 2010. Bounding surface plasticity model for the seismic liquefaction analysis of geostructures, *Soil Dynam Earthq Eng.* 30(10):895–911.

Arulmoli, K., Muraleetharan, K.K., Hossain, M.M., Fruth, L.S. 1992. VELACS: verifications of liquefaction analyses by centrifuge studies, *Laboratory testing program*. Soil Data Report.

Beaty, M., Byrne, P. M. 1998. An Effective Stress Model for Predicting Liquefaction Behavior of Sand, *Geotechnical Earthquake Engineering and Soil Dynamics III*, ASCE. Vol. 1, pp766 - 777.

Boulanger, R.W., Ziotopoulou, K. 2013. Formulation of a sand plasticity plane-strain model for earthquake engineering applications, *Soil Dynam Earthq Eng.* 53:254–67.

Cascone, E., G. Biondi, D. Aliberti, S. Rampello. 2021. Effect of vertical input motion and excess pore pressures on the seismic performance of a zoned dam. *Soil Dyn. Earthquake Eng.*, 142: 106566.

Chakraborty A, Sawant V.A. 2022. Numerical Simulation of Earthen Embankment Resting on Liquefiable Soil and Remediation Using Stone Columns, *International Journal of Geomechanics*, 22(11): 04022205-1 to 20.

Chakraborty, A., Sawant, V.A. 2022. Earthquake response of embankment resting on liquefiable soil with different mitigation models. *Natural Hazards*. https://doi.org/10.1007/s11069-022-05799-6.

Dinesh, N., and Banerjee, S. 2022. Rajagopal K. Performance evaluation of PM4Sand model for simulation of the liquefaction remedial measures for embankment, *Soil Dynam Earthq Eng.* 152: 107042.

Huang, D., G. Wang. 2017.Energy-compatible and spectrum-compatible (ECSC) ground motion simulation using wavelet packets. *Earthquake Eng. Struct. Dyn.*,46: 1855–1873.

Idriss, I.M., Boulanger, R.W. 2008. Soil liquefaction during earthquakes, *Monograph*. Earthquake Engineering Research Institute. 136(6): 755.

Kramer, S.L. 1996. Geotechnical earthquake engineering, Hoboken, NJ: Prentice-Hall.

Matsuo, O. 1996. Damage to river dikes, *Soils Found.* 235–40. Special.

McCulloch, D.S., Bonilla, M.G. 1967. Railroad damage in the Alaska earthquake, *J. Geotech. Eng. Div.* 93(5), 89–100.

NRC. 1985.Liquefaction of soils during earthquakes. *Report by the Committee on Earthquake Engineering Washington*, DC: National Research Council, National Academy Press.

Petalas, A., Galavi, V. 2013. Plaxis Liquefaction Model UBC3D-PLM. PLAXIS B.V.

Pubela, H., Byrne, M., Phillips, P. 1997. Analysis of canlex liquefaction embankments prototype and centrifuge models, *Canadian Geotechnical Journal.* 34:641-657.

Sriskandakumar, S. 2004. Cyclic loading response of fraser river sand for validation of numerical models simulating centrifuge tests, *Master of Applied Science thesis*, The University of British Columbia.

Taiebat, M., Dafalias, Y. F. 2008. SANISAND: simple anisotropic sand plasticity model, *Int J Numer Anal Methods GeoMech.* 32(32):915–48.

Tsegaye, A. 2010. Plaxis liqueafaction model. report no. 1. PLAXIS knowledge base.

Wang, G. 2012. Efficiency of scalar and vector intensity measures for seis-mic slope displacements. *Front. Struct. Civ. Eng.*, 6 (1): 44–52.

Yamada, G. 1966. Damage to earth structures and foundations by the Niigata earthquake, June 16, 1964, *Soils Found.* 6(1), 1–13.

Yang, Z., Elgamal, A., and Parra, E. 2003. Computational model for cyclic mobility and associated shear deformation, *J Geotech Geoenviron Eng.* 129(12):1119–27.